Biomedical Physics & Engineering Express

PAPER

Energy window optimization in bremsstrahlung imaging after Yttrium-90 microsphere therapy

C Kayaş Demirtaş[1], M Can[1,2], Ö Karadeniz[1,3], Ö Vupa Çilengiroğlu[4], T Ertay[1,5] and G Çapa Kaya[1,5]

[1] Department of Medical Physics, Institute of Health Sciences, Dokuz Eylül University, 35340, İnciraltı, İzmir, Turkey
[2] Program of Nuclear Medicine Techniques, Vocational School of Health Services, Dokuz Eylül University, 35330, İnciraltı, İzmir, Turkey
[3] Department of Physics, Faculty of Sciences, Dokuz Eylül University, 35390, Tınaztepe, Izmir, Turkey
[4] Department of Statistics, Faculty of Sciences, Dokuz Eylül University, 35390, Tınaztepe, Izmir, Turkey
[5] Department of Nuclear Medicine, Faculty of Medicine, Dokuz Eylül University, 35340, Inciraltı, Izmir, Turkey

E-mail: melek.can@deu.edu.tr

Keywords: Yttrium-90 TARE, bremsstrahlung imaging, energy window optimization, %FOV, image contrast, spatial resolution

OPEN ACCESS

RECEIVED
29 September 2023

REVISED
25 December 2023

ACCEPTED FOR PUBLICATION
2 February 2024

PUBLISHED
13 February 2024

Original content from this work may be used under the terms of the Creative Commons Attribution 4.0 licence.

Any further distribution of this work must maintain attribution to the author(s) and the title of the work, journal citation and DOI.

Abstract

In imaging of Yttrium-90 patients treated hepatic primary and metastatic cancers, bremsstrahlung photons produced in a wide energy range is used. However, the image quality depends on acquisition energy window. This research aimed energy window optimization for Yttrium-90 bremsstrahlung imaging and 48 patients with various types of cancer received radioembolization therapy were investigated. Patients were imaged using a GE Healthcare Optima NM/CT 640 series gamma camera system with a medium energy general-purpose (MEGP) collimator and planar images were acquired with 8 different energy windows in the 55–400 keV energy range. The data set, formed with the %FOV, contrast, and spatial resolution of image quality parameters calculated from these images, was statistically examined with ANOVA and Tukey tests. According to the visual evaluations and ANOVA/Tukey test results, it was statistically concluded that energy window of 90–110 keV is the optimal energy window while 60–400 keV energy ranges show the lowest image quality for Y-90 bremsstrahlung imaging.

1. Introduction

The most prevalent type of liver cancer is hepatocellular carcinoma (HCC). It is the fifth most common cancer in males and the seventh most common cancer in women globally. The hepatic artery supplies approximately 90% of the blood supply to HCC, while the portal venous system supplies 70% of the blood supply to normal liver parenchyma. Yttrium-90 transarterial radioembolization (^{90}Y-TARE) therapy is a transarterial method that uses the hepatic artery to deliver radioactive microspheres directly to tumors, causing cytotoxic damage [1, 2]. The safe delivery of high radiation doses to the tumor is made possible by selective intra-arterial injection of microspheres [3]. Imaging post-TARE is recommended in order to confirm the activity distributions of ^{90}Y microspheres in the patient body and to measure doses delivered to tumors and healthy organs [4, 5].

However, ^{90}Y imaging is not a straightforward process as commercially available gamma camera used for nuclear medicine imaging is designed for monoenergetic gamma-emitters. Unlike monoenergetic gamma-emitting medical radioisotopes with a pronounced photopeak (e.g., 140 keV energy photopeak for Technetium-99m (^{99m}Tc)), ^{90}Y is a pure beta emitter with a half-life of 2.67 days and mean energy of 0.93 MeV and has no primary gamma emissions. When the unstable Y-90 radioisotope decays, it emits a high-speed electron (beta particle) that causes targeted destruction of the target tumor, and bremsstrahlung photons are formed as a result of Y-90 beta particle interaction with body tissue.

One way to imaging of the ^{90}Y activity distribution in the patient's body is to take bremsstrahlung planar or single photon emission computed tomography (SPECT/CT) images [6]. Using bremsstrahlung photons allows for more accurate localization and identification of the spheres' intrahepatic and possibly extrahepatic distribution [7]. However, for therapies such as Y-90 transarterial radioembolization, the absence of monoenergetic gamma photons makes the

© 2024 The Author(s). Published by IOP Publishing Ltd



Figure 1. GE Healthcare, Optima NM/CT 640 SPECT/CT [15].

^{90}Y imaging more complex [8]. In ^{90}Y bremsstrahlung imaging, tissue attenuation, varying count rates of bremsstrahlung photons, low spatial resolution, continuous and wide spectrum acquisition, and the type of collimator used to affect the image quality [9, 10]. Moreover, the image quality shows differences depending on the energy window and energy window width used, due to the continuous energy spectrum and low efficiency of Y-90 bremsstrahlung photons. Therefore, Y-90 TARE post-treatment bremsstrahlung imaging is one of the most challenging issues in nuclear medicine.

Many experimental and simulation imaging studies have been conducted on the energy window selection in planar/SPECT bremsstrahlung imaging and detailed information was given in our previous study [11]. In a Y-90 bremsstrahlung imaging optimization study using a Monte Carlo code, the appropriate imaging condition was obtained with a High-Energy Medium-Resolution (HEMR) collimator in the energy range of 50–200 keV [4]. Huey *et al* (2020) evaluated the image quality parameters in a wide energy range of 60–300 keV using medium energy general purpose (MEGP), high energy general purpose (HEGP), and low energy high resolution (LEHR) collimators in the experimental phantom study, and it was determined that the optimum imaging condition was between 60–100 and 102–138 keV energy ranges with MEGP collimator. On the other hand, the highest image contrast was obtained with an energy window selection of 100–150 keV [12]. However, some studies have shown that there is no clear standard imaging protocol for ^{90}Y bremsstrahlung imaging with SPECT/CT [9, 13, 14].

In our previous study based on a Y-90 vial imaging with very high-count rates, optimum imaging parameters were obtained using HEGP collimator in the 90–110 keV energy range [11]. However, in the case of ^{90}Y bremsstrahlung imaging during patients' treatments, it is well known that the count rates are low. Therefore, there was a need to conduct an optimization study subjecting the patient imaging in Y-90 radioembolization therapy.

In the present study, energy window optimization for Yttrium-90 bremsstrahlung imaging was aimed. For this purpose, planar images were acquired with a gamma camera system using 8 different energy windows and the effects of energy windows on the image quality were evaluated statistically using the quality parameters such as % percentage of counts in the field of view (%FOV), spatial resolution and contrast.

2. Materials and methods

2.1. Imaging system and collimation

Patients were imaged using a GE Healthcare Optima NM/CT 640 series gamma camera system with a medium energy general-purpose (MEGP) collimator to improve the detection sensitivity of Yttrium-90 Bremsstrahlung photons in nuclear medicine imaging (figure 1). The system comprises of 59 photomultiplier tubes and two detectors with a 9.5 mm thick NaI(Tl) scintillation crystal. The system's MEGP collimator has a hole length of 58 mm, a diameter of 3 mm, a septal thickness of 1.05 mm and field of view 540 $\times$400 mm.

2.2. Yttrium-90 source

The source of Yttrium-90 TheraSphere® (MDS Nordion, Ottawa, Ontario, Canada) with 3–10 GBq activity given to patients for therapeutic purposes is glass spheres with an average size of 20–30 μm in a 1.0 ml glass vial placed in an acrylic armor (figure 2). One vial contains 22000–73000 microspheres/mL in 0.6 ml of sterile, apyrogen water.

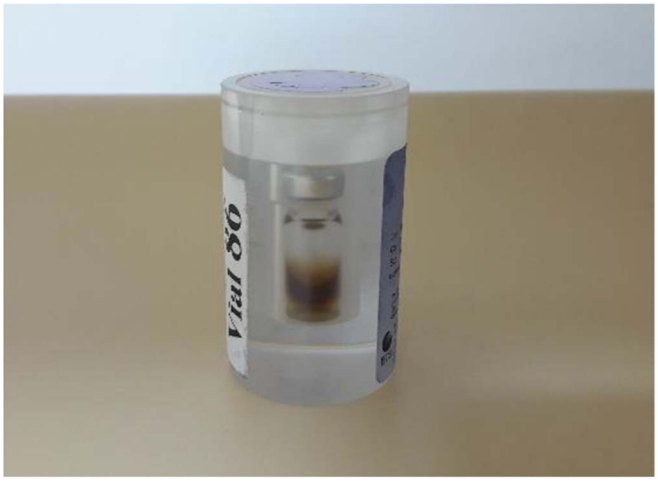


Figure 2. TheraSphere Y-90 glass microspheres [16].

2.3. Selection of yttrium-90 TARE patient

2.3.1. (Human study)

In this research, 48 patients with various types of cancer received radioembolization therapy were investigated. The mean ages of the patients included in the study were 61.75 ± 14.32 and 27.5 female (%) and 72.5 male (%). The study protocol was approved by the local ethics committee of Dokuz Eylül University.

2.4. Y-90 bremsstrahlung energy windows

In this energy window optimization study, planar images were acquired with 8 different energy windows in the 55–400 keV energy range (table 1). When selecting these energy windows, similar ^{90}Y imaging studies in the literature were considered. Because gamma camera systems can detect photons up to 55 keV, and high-energy photons (>500 keV) are subjected to septal penetration and scattering, this range was chosen for image quality.

2.5. Y-90 bremsstrahlung planar imaging

The yttrium-90 vials were tested in a dose calibrator before each radioembolization therapy and their activities were noted. TARE patients were positioned supine immediately following injection. Within 24 h of treatment, planar imaging was performed using two gamma camera detectors. The 'body-contour' tracking system was used for planar imaging in order to minimize the detector-patient distance, providing better resolution. Planar images were acquired at 2.40 mm pixels in 600 s.

2.6. Evaluation of the image quality

2.6.1. Region of interest (ROI)

In nuclear medicine imaging, a ROI definition is often required for quantitative evaluation of radioactive source uptake in the image. The choice of the ROI is the most essential factor when considering image quality parameters because it affects the count values. ROI is to draw the border of the volume of interest on each image slice, include the organ or tumor of related [14]. The total count in all pixels of the ROI is a measure of the activity in the patient's related region [17].

In the study, five circular source ROIs were drawn to include a total activity region in the anterior and posterior planar images of the liver. The five background (BG) ROIs were drawn around the liver also. On the images, care has been made to ensure that the source and BG ROI regions (number of pixels) were the same.

Table 1. Energy windows investigated for Yttrium-90 bremsstrahlung imaging.

No	Energy (keV)[a]	%[b]	E_1-E_2 (keV)	ΔE (keV)[c]
1	75	50	56–94	38
2	100	49,5	75–125	50
3	100	20	90–110	20
4	152,5	128	55–250	195
5	90	30	77–104	27
6	80	15	74–86	12
7	75	16	69–81	12
8	230	74	60–400	340

[a] Centered Energy.
[b] Energy-window width (%).
[c] Energy-window width (keV).

2.6.2. Percentage of counts in the field of view (%FOV)

The useful field of view count percentage (%FOV) parameter is used to evaluate bremsstrahlung photon scatter on planar images [18]. For the purpose of assessing the impact of scattering, the counts in the source ROI are stated as a percentage of the FOV. Greater %FOV values indicate less photon scattering. The %FOV value is calculated by the equation below:

$$\%FOV = \frac{Counts\ \ in\ \ the\ \ source\ \ ROI}{Total\ \ count\ \ in\ \ the\ \ FOV} \times 100 \quad (1)$$

2.6.3. Image contrast

One of the conventional methods of measuring image quality is contrast calculation which is a measurement of how easily abnormal tissue may be distinguished from surrounding tissue in an image. The greater the difference between the concentrations in normal and abnormal tissue, the easier it is to detect anomalies such as lesions in the tissue. Factors such as count density, image noise caused by background activity, size of the lesion and patient movement can affect the contrast of the image [19]. The contrast value for an image can be expressed by equation (2):

$$Contrast = \frac{C_{Source} - C_{BG}}{C_{BG}} \quad (2)$$

where C_{source} (counts/pixel) is count read in the source ROIs and C_{BG} (counts/pixel) is the average count read in the background ROIs.

2.6.4. Spatial resolution (FWHM—full width at half maximum)

The spatial resolution parameter, which is one of the most important image quality characteristics, is read from the profile curves drawn on the source images [20]. In order to determine the spatial resolution, the full width at the half maximum (FWHM) of the profile of a point or linear radiation source is usually used [21, 22]. In the study, rectangular profile ROIs were drawn in the center of each source ROI using the 'Xeleris 4.0 Processing & Review' workstation on all planar images (figure 3(a)). In all patient planar anterior-posterior views, FWHM values were read from the profile curves obtained for each source ROI (figure 3(b)).

2.7. Statistical analysis

The study involved obtaining image quality parameter values for three variables (contrast, %FOV, and spatial resolution) from anterior and posterior liver images in 8 different energy windows, with 6 observations for each window. Additionally, anterior and posterior liver images were examined in three different areas (averages of total anterior and posterior values, only anterior values, and only posterior values). For each area, normality test (Kolmogorov-Smirnov) was applied to the data composing the variables on an energy window basis. Subsequently, an ANOVA test was conducted to identify statistically significant differences among the means of window data for the three variables in each area.

Tukey, one of the multiple comparison tests, was used to show the difference between the energy windows according to the results of the ANOVA test. Within the study, alpha values were determined as 0.05 and 0.10.

3. Results and discussion

3.1. Y-90 bremsstrahlung spectrum

In this paper, choice of acquisition energy window on image quality was evaluated by bremsstrahlung images of Y-90 TARE patients using a MEGP collimator and 8 different energy windows (55–400 keV). The figure 4 shows an example of Y-90 Bremsstrahlung energy spectrum acquired with MEGP collimator and energy window with of 90–110 keV. As expected, ^{90}Y bremsstrahlung photons have a continuous and broad energy distribution in the energy range from 0 to 500 keV [11]. The characteristic lead x-ray peak, shown in the 70–90 keV energy range is results of the interaction between bremsstrahlung photons and the lead collimator.

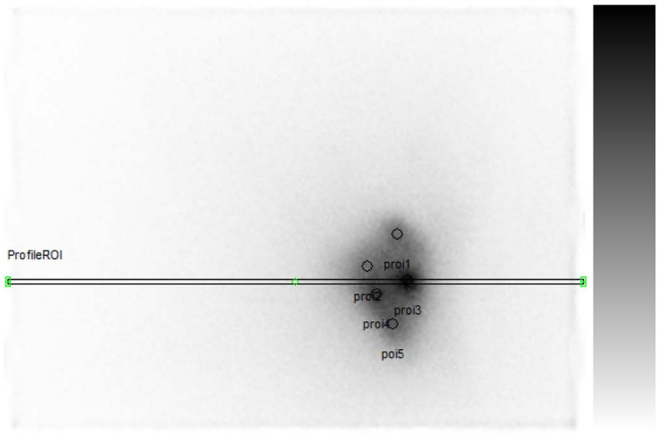
3.2. Y-90 bremsstrahlung imaging

Within the scope of the study, liver images were obtained with the MEGP collimator gamma camera system after treatment of Y-90 RE patients. The effects of the energy window on image quality are clearly seen in the anterior liver images acquired with energy windows listed in table 1 (figure 5). For example, artifacts in the 55–250 keV energy window are not seen in the 90–110 keV energy window. Considering all the energy windows in the visual evaluation, it is clearly seen that the wide selection of energy windows, such as 55–250 and 60–400 keV distorts the image and increases the background activity. On the other hand, when planar images are compared, it is seen that figures 5(c), (f), (g) have more distinct lesion borders and a homogeneous background compared to other liver images.

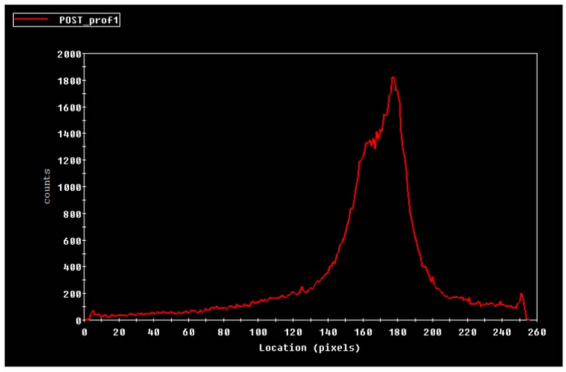
3.3. Y-90 image quality parameters

In the study, image quality parameters of %FOV, contrast and spatial resolution were calculated for liver images and compared in order to determine the optimum energy window. The data collected from the anterior and posterior images were averaged throughout these calculations, in order to ensure that the results are not affected by differences caused by anterior and posterior imaging (figure 6).

The normality of the data obtained for the %FOV, contrast and spatial resolution parameters from the anterior and posterior images was evaluated with the Kolmogorov- Smirnov test (H0: 'anterior and posterior' value in the %FOV, contrast, spatial resolution parameter, the data for the xth energy window are normal, x = 1, 2,…,8, $p < 0.10$). According to the results of this test, since H0 could not be rejected in all energy window data for these parameters, it was accepted that the data came from a statistically normal distribution. ANOVA test was used to find a statistical difference between the means of the parameters obtained from the anterior and posterior images. Tukey test was performed to show the difference between energy windows.



(a)



(b)

Figure 3. (a) Profile ROIs drawn on the anterior liver image of Y-90 TARE patient (b) Profile curves plotted from profile ROIs.

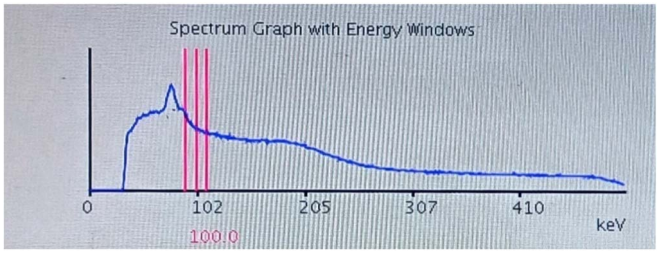


Figure 4. Y-90 Bremsstrahlung energy spectrum acquired with the gamma camera system equipped with MEGP collimator. The energy window width of 20% (90–110 keV) centered at 100 keV was set on the spectrum.

3.3.1. % FOV

The bremsstrahlung scattering effects on the images of Y-90 TARE patients were evaluated using the %FOV calculation given in equation (1). Accordingly, the highest %FOV value was obtained as 0.78% for the 90–110 keV energy window. The lowest %FOV value was found as 0.43% in the 60–400 keV energy window (figure 6). This finding was also supported by visual evaluation shown in figure 5(h) with high background area. Therefore, the poor image taken with 60–400 keV energy range can be attributed to a high level of scattering effects.

According to the results of the ANOVA test, a statistically significant difference was found between the means of the %FOV parameter for different energy windows with 95% confidence level ($p = 0.028 < 0.05$). Although there was a statistically significant difference between only the two energy windows (90–110 keV and 60–400 keV ($p = 0.024 < 0.05$)), when the Tukey mean graphs were examined, it was clear that the 90–110 keV energy window gave a better image when compared to other energy ranges (figure 7).

3.3.2. Image contrast

Contrast is one of the most traditional parameters of evaluating the image quality. Calculations were made for each image acquired with a studied energy window using equation (2). Accordingly, maximum contrast

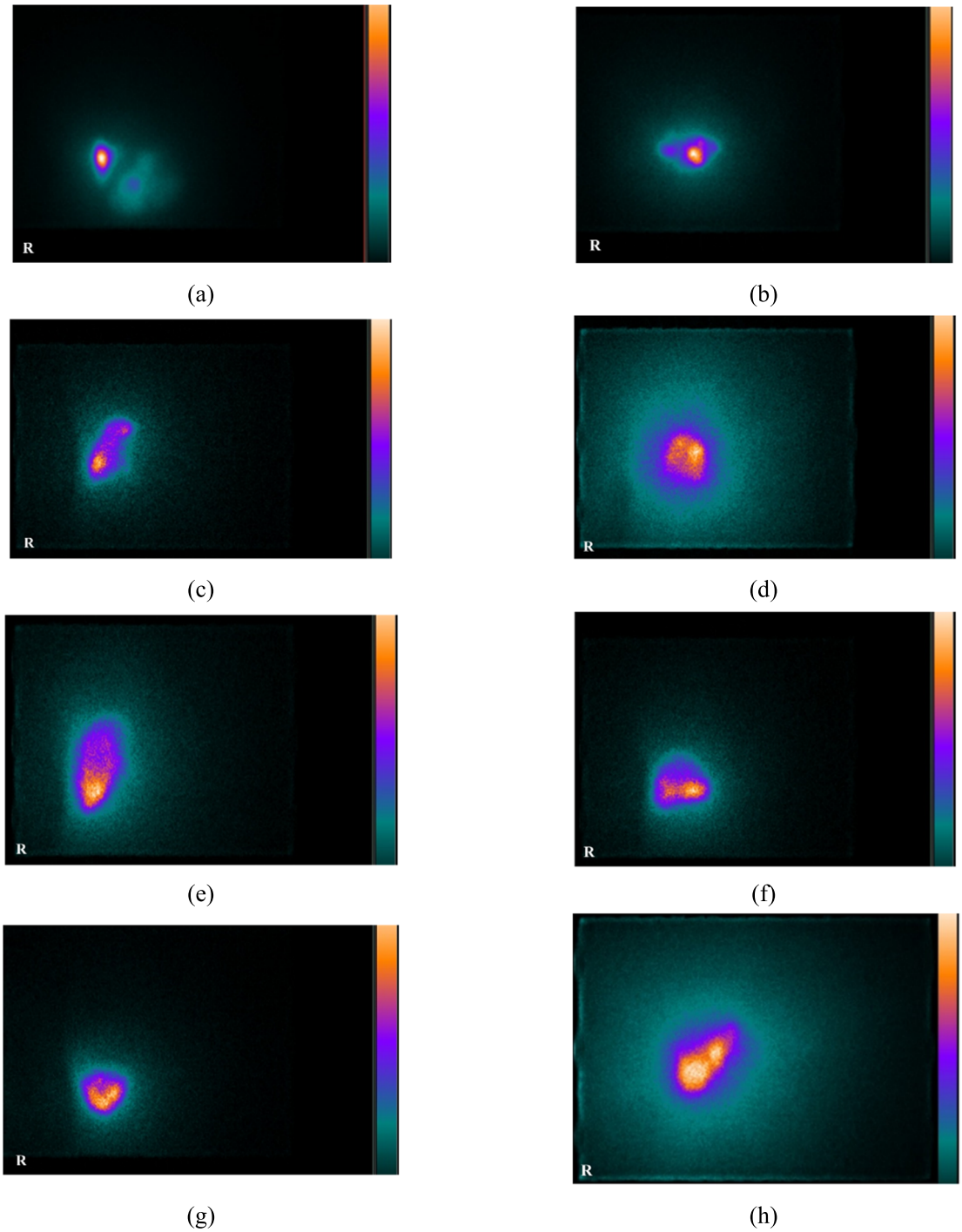


Figure 5. Y-90 planar images of the liver taken for (a) 56–94 keV, (b) 75–125 keV, (c) 90–110 keV, (d) 55–250 keV, (e) 77–104 keV, (f) 74–86 keV, (g) 69–81 keV and (h) 60–400 keV energy windows.

had a value of 4.46 for the 90–110 keV energy window and a minimum contrast value of 2.07 found for the 60–400 keV energy window.

Results of the ANOVA test show that a statistically significant difference was found between the means of the contrast parameter for different energy windows with 95% confidence level ($p = 0.013 < 0.05$). Although the 'contrast' parameter for 90–110 keV energy window is statistically different only from the energy windows of 60–400 keV (Tukey, $p = 0.005 < 0.05$) and 77–104 keV (Tukey, $p = 0.063 < 0.10$), it has been clearly shown from the graph obtained from the ANOVA that the 90–110 keV energy window gives a better image than other energy windows (figure 8).

3.3.3. Spatial resolution (FWHM—full width at half maximum)

In the study, the spatial resolution parameter is considered as the FWHM parameter read from the profile curves, and plotted profile curves are presented in figure 8. In this figure, the profile curves corresponding to the five source ROIs mentioned in figure 3

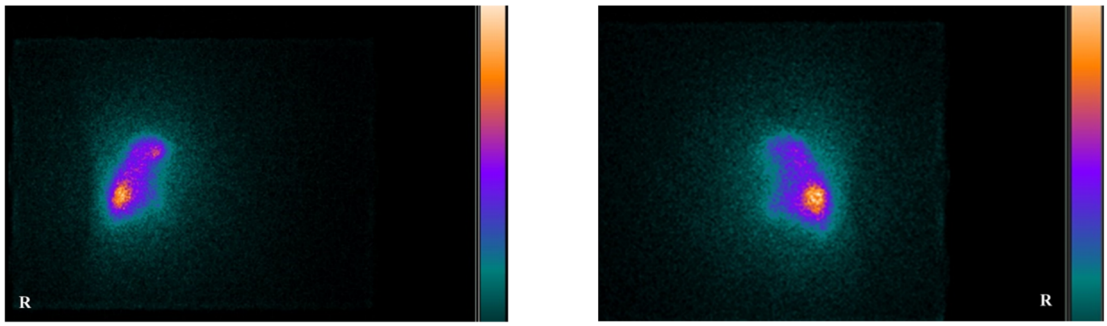


Figure 6. Y-90 planar images of the (a) anterior (b) posterior liver taken for 90–110 keV energy window.

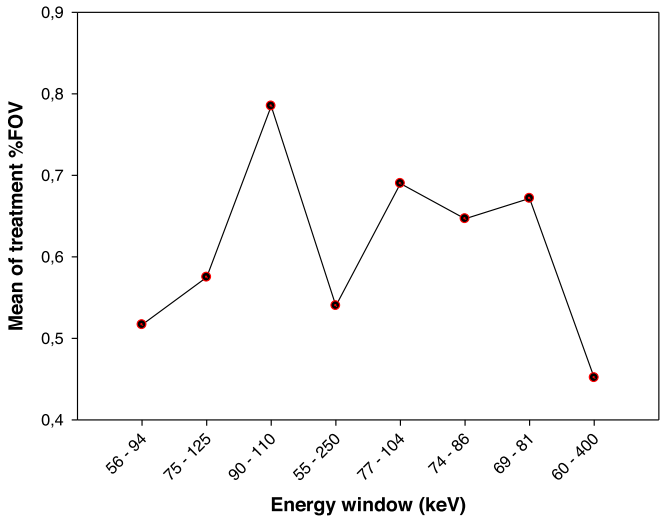


Figure 7. ANOVA means plot for %FOV parameter according to the energy windows.

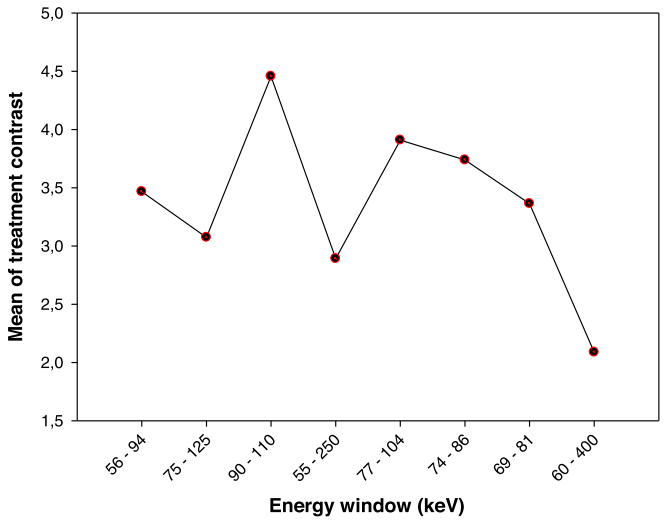


Figure 8. ANOVA means plot for contrast parameter according to the energy windows.

are shown with five different colors. The variations on the Yttrium-90 images caused by the different energy windows can also be seen in the profile curves, which have a Gaussian distribution (figure 9). From the profile curves, the highest FWHM value was obtained as 45.8 mm for the 56–94 keV energy window, while the lowest FWHM value was found as 29.7 mm for 90–110 keV energy window. The measured value

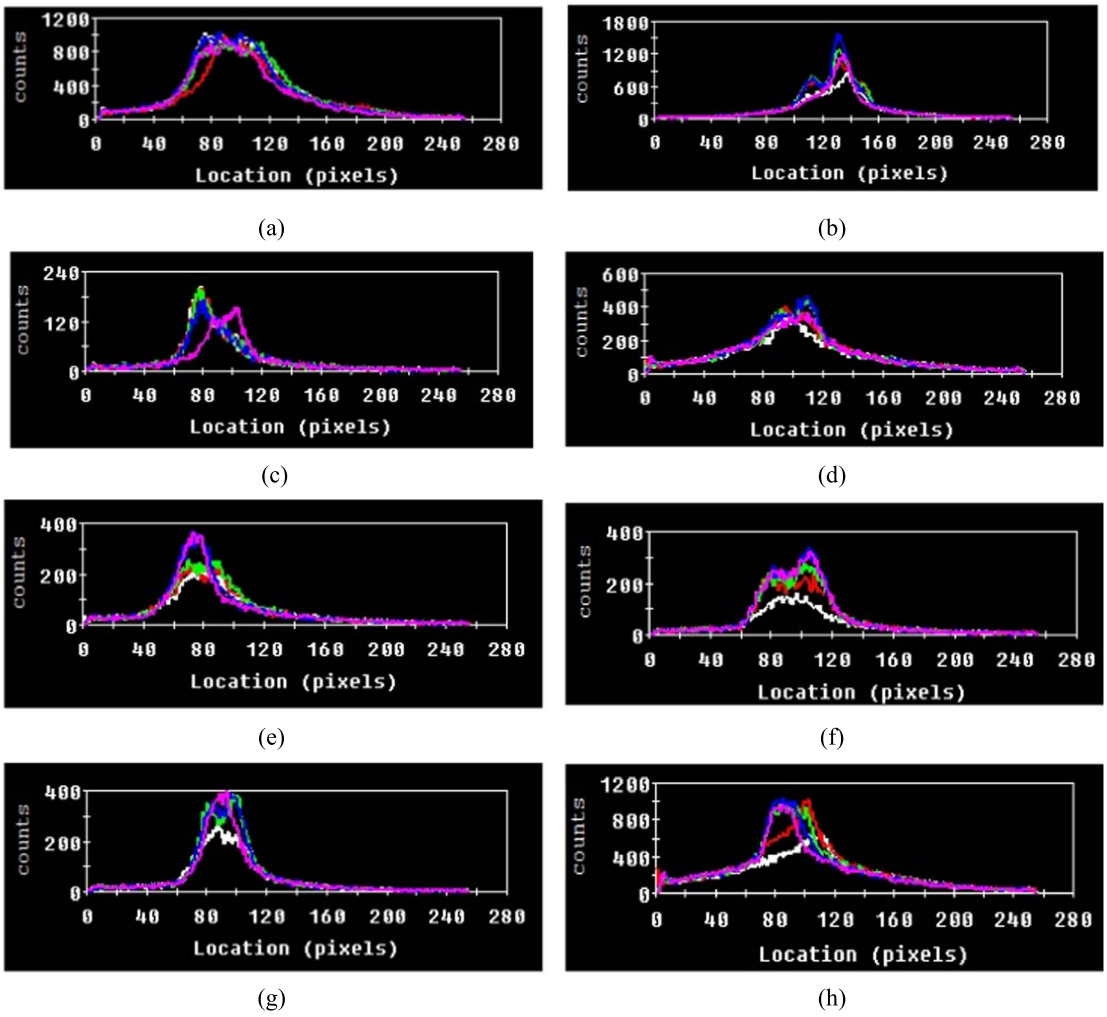


Figure 9. Profile curves with five different color corresponding to the five source ROIs for the energy windows of (a) 56–94 keV, (b) 75–125 keV, (c) 90–110 keV, (d) 55–250 keV, (e) 77–104 keV, (f) 74–86 keV, (g) 69–81 keV and (h) 60–400 keV.

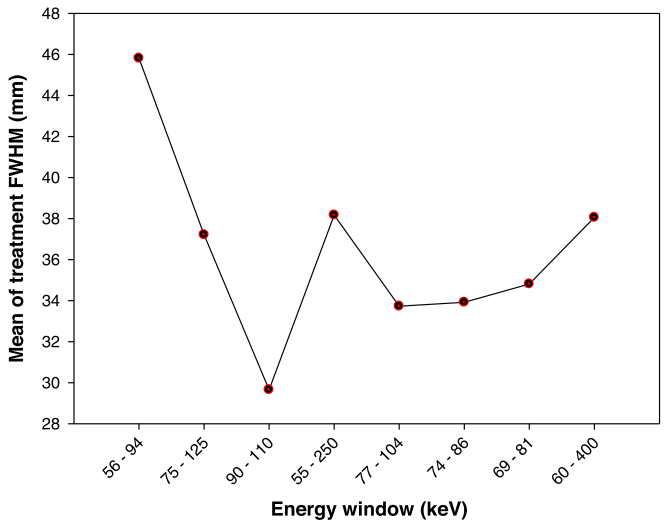


Figure 10. ANOVA means plot for FWHM according to the energy windows.

reported is an average based on the shape of the distribution data. The width of the distribution is a measure of the precision of the measurement also. According to this, it is seen that the profile curves for the 55–250 keV and 60–400 keV energy ranges are broad. Thus, it is concluded that the higher FWHM

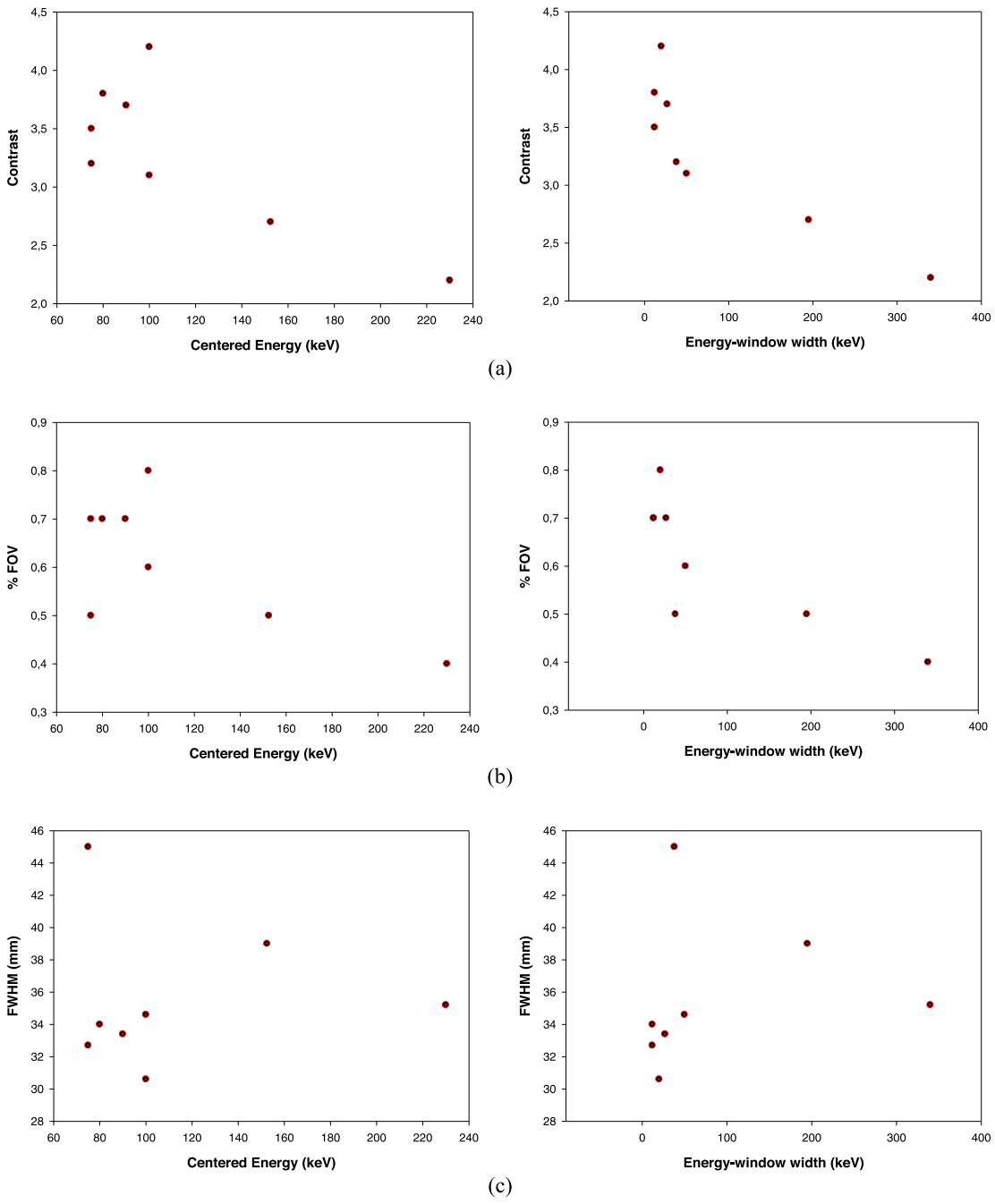


Figure 11. Plots for centered energy and energy-window width according to the (a) contrast (b) % FOV (c) spatial resolution (FWHM) parameters.

values were found for the energy windows with poor images in the visual evaluation.

According to the results of the ANOVA test, a statistically significant difference was found between the means of the FWHM values for different energy windows with 90% confidence level ($p = 0.071 < 0.10$). Although there is a statistically significant difference only for the 90–110 keV and 56–94 keV energy windows for the 'FWHM' value (Tukey, $p = 0.025 < 0.05$), it has been clearly demonstrated by the ANOVA means plot that the 90–110 keV energy window gives a better image than the other energy windows (figure 10).

3.4. Optimal imaging conditions for planar images

In this study aimed Y-90 TARE bremsstrahlung imaging optimization, liver images were evaluated both visually and statistically. For this purpose, the data sets used in the examination of TARE liver images were statistically analyzed by considering the %FOV, contrast and spatial resolution of traditionally image quality parameters.

According to the visual evaluations and ANOVA/Tukey test results, it was statistically concluded that energy window of 90–110 keV is the optimal energy window while 60–400 keV energy ranges show the lowest image quality for Y-90 bremsstrahlung

imaging. These ranges are consistent with other investigations related energy window optimization with medium energy collimator [6, 8, 12, 13]. Namely, due to the Y-90 Bremsstrahlung energy spectrum has large numbers of low-energy photons, it is concluded that 50–100 keV energy window is the most proper energy window when using the medium energy collimator [23]. Spectral components of 225–300 keV and 300–400 keV in 90Y bremsstrahlung spectrum correspond the region of backscatter, collimator scatter and septal penetration [13]. For example, it is reported that the fraction of detected photons undergoing septal penetration for a 400–450 keV window is much larger than for a 100–150 keV window [24]. It is reported that energy window conditions with wider ranges of energy width (60–400 keV) cause higher FWHM, as a result of more unexpected photons [8]. As a summary of the above, effect of energy region and energy-window width on the image quality parameters found in this study can be seen from figure 11. Thus, the region of the spectrum with the greatest proportion of unscattered photons and the collimators with a small amount of septal scatter and penetration are recommended for reliable 90Y Bremsstrahlung imaging [24]. Nevertheless, some simulation studies concluded that the optimal energy window was 60–400 keV for ^{90}Y bremsstrahlung SPECT imaging is also available [24–26].

It should also be said that a medium energy collimator was used for Y-90 bremsstrahlung imaging in this study and results may vary if a high energy collimator is used. Since the low count of bremsstrahlung photons is the main problem in Y-90 imaging, in case of using high energy collimator, wider ranges of energy width can be resulted in images with an appropriate combination of sensitivity and quality [8, 23].

4. Conclusion

After Y-90 TARE treatment, imaging is significant for assessing the distribution of microspheres. However, the planar image quality of Y-90 patients has poor because of the bremsstrahlung photon spectrum that has not a distinct photopeak. Therefore, choice of the ideal acquisition energy range in Y-90 imaging is very important and a more complex issue in the field of nuclear medicine for many years in radionuclide therapy and dosimetry processes.

In our previous Y-90 imaging study performed with the Y-90 vial, it was concluded that the best image was obtained in the 90–110 keV energy range. However, the count rate was extremely high because vials with 3–7 GBq of activity were viewing in the study. As the count rates in Y-90 TARE patients' imaging were low, it was necessary to perform an optimization study for low-count rates.

In the present study, planar TARE liver images were acquired with a gamma camera system using 8 different energy windows and the data set formed with the % FOV, contrast, and spatial resolution parameters calculated from these images was statistically examined with ANOVA and Tukey tests. An ideal bremsstrahlung imaging for Y-90 TARE patients is achieved with an energy window of 90–110 keV.

Even though this work reported here is an experimental attempt to choosing ideal acquisition energy range for post planar imaging in ^{90}Y radioembolization therapy, it should be said that the collimator used in bremsstrahlung imaging has a major impact on the image quality also. In addition, imaging conditions such as imaging time and timing, patient motion and the activity of the ^{90}Y source may also have a significant effect on image quality. Furthermore, the energy window optimization should be performed to SPECT (3D imaging) especially for voxel-based dosimetry. Attenuation correction, image filtering, reconstruction are another challenging topics in optimizing ^{90}Y bremsstrahlung SPECT imaging. Therefore, further phantom studies based on ^{90}Y bremsstrahlung SPECT imaging that aimed to optimize the energy window and collimation must be performed.

And finally, the conclusion from the above mentioned is that there is no single standardized imaging protocol due to the specific characteristics of the imaging system in each center. As a result, it is recommended to perform the imaging optimization specific to imaging systems.

Acknowledgments

Authors are grateful to the staff of Nuclear Medicine Department at Dokuz Eylül University for their encouragement and strong collaboration in the course of the measurement campaign. The authors are also grateful to two anonymous reviewers for their constructive suggestions and critiques.

Data availability statement

All data that support the findings of this study are included within the article (and any supplementary files).

Funding

This research did not receive any specific grant from funding agencies in the public, commercial, or not-for-profit sectors.

Declaration of competing interest

The authors declare that they have no known competing financial interests or personal relationships that could have appeared to influence the work reported in this paper.

ORCID iDs

M Can https://orcid.org/0000-0002-9969-2566
Ö Karadeniz https://orcid.org/0000-0001-7374-4527
Ö Vupa Çilengiroğlu https://orcid.org/0000-0003-0181-8376
T Ertay https://orcid.org/0000-0003-4206-6836
G Çapa Kaya https://orcid.org/0000-0002-1256-7325

References

[1] Geschwind J F H, Salem R, Carr B I, Soulen M C, Thurston K G, Goin K A, Buskirk M V, Roberts C A and Goin J E 2004 Yttrium-90 microspheres for the treatment of hepatocellular carcinoma *Gastroenterology* **127** 5194–205
[2] Saini A, Wallace A, Alzubaidi S, Knuttinen M G, Naidu S, Sheth R, Albadawi H and Oklu R 2019 History and evolution of yttrium-90 radioembolization for hepatocellular carcinoma *J. Clin. Med.* **8** 55
[3] Kallini J R, Gabr A, Salem R and Lewandowski R J 2016 Transarterial radioembolization with yttrium-90 for the treatment of hepatocellular carcinoma *Adv. Ther.* **33** 699–714
[4] Talebi A S and Rajabi H 2021 Developing a protocol for ^{90}Y bremsstrahlung imaging after transarterial radioembolization *J. Instrum.* **17** P03019
[5] Uribe C F, Esquinas P L, Gonzalez M and Celler A 2016 Characteristics of Bremsstrahlung emissions of (177) Lu, (188) Re, and (90)Y for SPECT/CT quantification in radionuclide therapy *Phys. Med.* **32** 691–700
[6] Huey O S, See Y J, Nabila S, Ping H S and Suzanah I 2020 Collimator and energy window optimization for practical imaging protocol and quantification of Yttrium-90 bremsstrahlung spect/ct: a phantom study *Radiat. Phys. Chem.* **178** 109080
[7] Ahmadzadehfar H, Duan H, Haug A R, Walrand S and Hoffman M 2014 The role of SPECT/CT in radioembolization of liver tumours *Eur. J. Nucl. Med.* **41** (Suppl 1) S115–24
[8] Kim H, Fessler J A, Wilderman S J, Brooks A F and Dejawara Y K 2019 Y-90 SPECT ML image reconstruction with a new model for tissue-dependent bremsstrahlung production using CT information: a proof-of-concept study *Phys. Med. Biol.* **63** 115001
[9] Wright C L, Zhang J, Tweedle M F, Knopp M V and Hall N C 2015 Theranostic imaging of yttrium-90 *Bio. Med. Res. Int.* **2015** 481279
[10] Padia S A, Alessio A, Kwan S W, Lewis D H, Vaidya S and Minoshima S 2013 Comparison of positron emission tomography and bremsstrahlung imaging to detect particle distribution in patients undergoing yttrium-90 radioembolization for large hepatocellular carcinomas or associated portal vein thrombosis *Journal of Vascular and Interventional Radiology* **24** P1147–53
[11] Ince C, Karadeniz Ö, Ertay T and Durak H 2021 Collimator and energy window optimization for YTTRIUM-90 bremsstrahlung SPECT imaging *Appl. Radiat. Isot.* **167** 109453
[12] Heard S, Flux G D, Guy M J and Ott R J 2004 Monte Carlo simulation of 90Y Bremsstrahlung imaging *IEEE Symposium Conference Record Nuclear Science* **6** 3579–83
[13] Siman W, Mikell J K and Kappadatha S C 2016 Practical reconstruction protocol for quantitative 90Y bremsstrahlung SPECT/CT *Med. Phys.* **43** 5093–103
[14] Bailey D L, Humm J L, Pokropek A T and van Aswegen A 2014 *Nuclear Medicine Physics: A Handbook for Teachers and Students* 1st edn (International Atomic Energy Agency)
[15] Can M, Karadeniz Ö, Çapa Kaya G and Ertay T 2023 A study on energy window-based scatter correction methods in 99mTc and 123I imaging *J. Instrum.* **18** P10009
[16] Ince C 2019 Collimator and Energy Window Optimization on Yttrium-90 Imaging *MSc Thesis Dokuz Eylül University* (Turkish with English abstract)
[17] Bushberg J T, Seibert J A, Leidholdt E M and Boone J M 2012 *The Essential Physics of Medical Imaging* 3rd edn (Lippincott Williams & Wilkins)
[18] Shen S, DeNardo G L, Yuan A, DeNardo D A and DeNardo S J 1994 Planar gamma camera imaging and quantitation of Yttrium-90 bremsstrahlung *J. NucI. Med.* **35** 1381–9
[19] Saha G B 2013 *Physics and Radiobiology of Nuclear Medicine* (Springer Science+Business Media)
[20] Cecchin D, Poggiali D, Riccardi L, Turco P, Bui F and Marchi S D 2015 Analytical and experimental FWHM of a gamma camera: theoretical and practical issues *PeerJ.* **3** e722
[21] Cherry S R, Sorenson J A and Phelps M E 2012 *Physics in Nuclear Medicine* (Saunders Elsevier Inc.)
[22] Zaidi H 2016 *Quantitative Analysis in Nuclear Medicine Imaging* 1st edn (Springer)
[23] Talebi A S and Rajabi H 2022 Developing a protocol for 90Y bremsstrahlung imaging after transarterial radioembolization *J. Instrum.* **17** P03019
[24] Rong X, Ghaly M and Frey E C 2013 Optimization of energy window for 90Y bremsstrahlung SPECT imaging for detection tasks using the ideal observer with model-mismatch *Med. Phys.* **40** 062502
[25] Taherparvar P and Shahmari N 2019 Effect of ME collimator characteristic, energy window width, and reconstruction algorithm selection on imaging performance of yttrium-90: simulation study *Nuclear Medicine and Molecular Imaging* **53** 414–22
[26] Roshan H R, Mahmoudian B, Gharepapagh E, Azarm A and Islamian J P 2016 Collimator and energy window optimization for 90Y bremsstrahlung SPECT imaging: a SIMIND Monte Carlo study *Appl. Radiat. Isot.* **108** 124–8